Nanocontainer-Based Anticorrosive Coatings: Effect of the Container Size on the Self-Healing Performance

Dimitriya Borisova, Dilek Akçakayıran, Matthias Schenderlein, Helmuth Möhwald, and Dmitry G. Shchukin*

Organic coatings based on inhibitor loaded inorganic containers for smart corrosion inhibition are presented. The overall coating performance is strongly influenced by the containers as well as their inhibitor capacity, compatibility with the coating matrix, and size. The important effect of container size is described for the first time in this work by investigating two types of mesoporous silica containers of different diameters: 80 and 700 nm. The coating physical properties (thickness and adhesion) are comparable for both container types. In contrast, the coating barrier properties are strongly influenced by the container size as assessed with electrochemical impedance spectroscopy (EIS). The incorporation of bigger containers reduces the coating resistance by a factor of two. Surprisingly, despite the similar amounts (20 wt%) of loaded inhibitor (2-mercaptobenzothiazole), different active inhibition ability is detected with the scanning vibrating electrode technique (SVET). Therefore, it is found that coatings with smaller containers exhibit better self-healing performance.

1. Introduction

The main function of anticorrosive coatings is to protect the underlying metal from corrosive attack. The major drawback of these coatings is that they lose their protective function when they are damaged, i.e., they provide only passive protection.[1] In contrast, active anticorrosive coatings protect the underlying metal from corrosion even when they are not intact.[2] Imparting such a functionality is possible by the addition of nano-/microcontainers containing corrosion inhibitor.[3] This is a promising approach to isolate the inhibitor from the coating components and to incorporate it homogeneously in high amounts. An optimum coating has to provide not only sufficient active corrosion protection but also barrier function, good adhesion and mechanical strength. This is studied in total in this work.

Dr. D. Borisova, Dr. D. Akçakayıran, Dr. M. Schenderlein, Prof. H. Möhwald, Dr. D. G. Shchukin
Max Planck Institute of Colloids and Interfaces
Am Mühlenberg 1, 14424 Potsdam-Golm, Germany
E-mail: borisova@mpikg.mpg.de
D. G. Shchukin
Stephenson Institute for Renewable Energy
Department of Chemistry
The University of Liverpool
L69 4ZF Liverpool, UK

DOI: 10.1002/adfm.201203715

Anticorrosive coatings based on inhibitor loaded containers function as feedback active systems and self-recover their anticorrosive, protective function. This is realized by releasing corrosion inhibitor in response to changes in the coating integrity (cracks) or local environment (pH shift) caused by corrosion attack. These self-healing systems have been extensively investigated, because they are potential replacements of the banned chromate-based coatings. Various types of containers for inhibitor encapsulation have been reported so far. These differ in their size (nano- and microcontainers), chemical nature (organic, inorganic), shape (spheres, tubes, platelets) and structure (core-shell, porous, layered).[4] This huge variety implies also different possible stimuli for inhibitor release (pH shift, ion exchange or mechanical rupture) resulting in numerous anticorrosive coating designs.[5]

Utilizing pH shift as stimulus for corrosion inhibitor release is the natural and the most promising approach to design anticorrosive coatings with sufficient corrosion resistance. That is because the corrosion process leads to local pH decrease in anodic areas and local pH increase in cathodic ones.[6] Therefore, integrating pH sensitive inhibitor capsules in the coating is an attractive approach to sense and to eliminate the negative impact of corrosion.

One way to form such capsules is by the layer-by-layer (LbL) assembly of oppositely charged species (e.g., polyelectrolytes) on templating dense or porous metal oxide nanoparticles.[7–11] However, the complex design of such nanocontainers restricts their up-scaling. This led to the development of simpler containers without protective shell or stoppers.[12–15] The biggest drawback of these containers is the low amount of loaded inhibitor (≈5 wt%) that limits the long-term anticorrosion performance.

This disadvantage could be overcome for organic coatings by using porous organic microcapsules formed by emulsion polymerization[16] or nanoparticle stabilized polymer nanocontainers based on Pickering emulsions.[17] The achieved loading was 45 wt% for the liquid inhibitor (2-methylbenzothiazole) and 20 wt% for solid inhibitor (8-hydroxyquinoline). Unfortunately, organic micro-/nanocontainers of this type have the following significant restrictions: i) the inhibitor can interact negatively with the containers resulting in its deactivation, ii) the

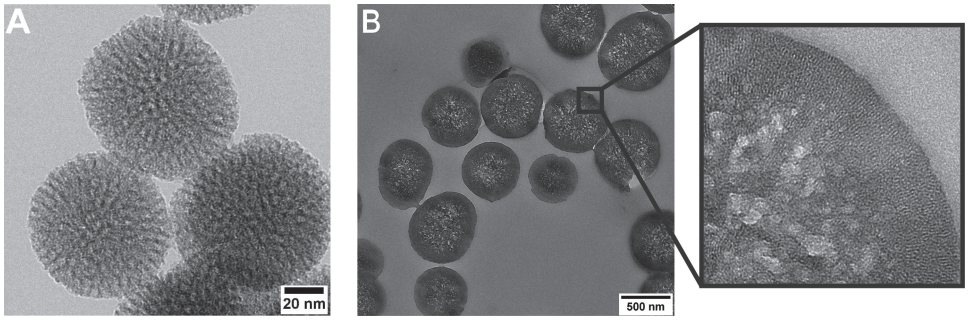

Figure 1. TEM images of a) mesoporous silica nanocontainers (NCs) and b) microtomed spherical hollow silica containers (SHS); the zoomed image reveals the pore structure of SHS.

container loading efficiency is limited to the inhibitor solubility in the emulsion oil phase forming the container core, and iii) the inhibitor release is not controlled and prolonged, limiting long-term corrosion inhibition.

An attractive alternative to the containers described above is mesoporous inorganic particles. We have recently shown that mesoporous silica particles (MSP) with large pore volume (≈1 mL g^{-1}) and surface area (≈1000 m^2 g^{-1}) can be used as nanocontainers for organic inhibitors. Employing these MSP a two times greater inhibitor uptake was achieved.[18–20] The incorporation of mesoporous nanocontainers into inorganic, sol-gel coatings improved significantly the coating corrosion resistance. On one hand, the coating barrier properties were improved by reinforcement of the coating matrix due to introduction of mechanically stable, robust silica nanoparticles. On the other hand, the large amount of encapsulated inhibitor and its controlled release upon corrosion attack provided superior active corrosion inhibition.

The incorporation of porous silica nanoparticles into organic coatings was not shown before and is still a new topic. Distributing sufficiently high amount of inhibitor loaded containers in the coating matrix while preserving its integrity is a challenging task. Its accomplishment requires a careful choice of the container concentration and size. The influence of these important parameters on the anticorrosion performance of organic coatings is described for the first time in the present work. To study the size effect of the embedded containers, two types of porous silica containers with $d_1 \approx 80$ and $d_2 \approx 700$ nm were embedded in a 20 µm thick, water-based epoxy coating. The barrier properties and self-healing ability of the studied coatings were evaluated by electrochemical impedance spectroscopy (EIS) and scanning vibrating electrode technique (SVET), respectively.

2. Results and Discussion

2.1. Mesoporous Silica Containers

In this work we synthesized and compared two types of porous silica containers: i) mesoporous silica nanocontainers (NCs) and ii) spherical hollow silica microcontainers (SHS). Dynamic light scattering, SEM and TEM measurements showed that the container diameters differ by one order of magnitude: $d_{NCs} \approx 80$ nm and $d_{SHS} \approx 700$ nm. The NCs were described in detail in our previous work.[19] The investigation of the synthesized silica containers with electron microscopy (SEM and TEM) confirms the monodispersity of the samples (**Figure 1** and Figure S1 in the Supporting Information). Both container types exhibit spherical shape and rough surface. The shape preservation of the particles after the mechanical stress during the synthesis steps indicates their structural stability. The TEM micrographs of the NCs reveal open, cylindrical pores growing from the centre to the periphery of the particles (Figure 1a). The TEM analysis of microtomed SHS reveals their core-shell porous character (Figure 1b). The shell is around 100 nm thick with worm-like mesopores ordered in short range parallel to each other. The core is more porous with disordered cage-like, round pores of diameter around 25 nm.

The porosity of the silica containers was evaluated with N_2 sorption measurements, which delivered a type IV isotherm for both container types (Supporting Information Figure S2). For the NCs a BET surface area of ≈1000 m^2 g^{-1} and a cumulative pore volume of ≈1.2 mL g^{-1} were determined. The worm-like, cylindrical pores have a narrow size distribution with a distinct peak having a maximum at 4 nm (Supporting Information Figure S2b). The N_2 sorption isotherms obtained for the spherical hollow silica containers (SHS) display a distinct hysteresis loop of type H2 in the p/p_0 range of 0.4–1.0 (Supporting Information Figure S3a).[21] This is an indication of the presence of wide bodied pores with narrow necks. As revealed by the TEM analysis of SHS (Figure 1b) the container core consists of bigger cage-like pores and the shell contains smaller cylindrical mesopores. Thus, the H2 hysteresis loop, which is typical for silica particles synthesized by the emulsion method, can be assigned to the porosity of the SHS core.[22] Despite the different morphology of the studied containers, the surface area of the SHS is similar to the NCs one (≈1000 m^2 g^{-1}). The pore size distribution curve of the SHS obtained using the non-local density functional theory (NLDFT) model for cylindrical pores and the adsorption branch reveals one sharp peak, indicating a narrow pore size distribution with average pore width of ≈3 nm (Supporting Information Figure S3b). This pore width is in agreement with the TEM observations. The pore volume of the SHS was calculated to be ≈0.8 mL g^{-1}, which classifies the SHS as an attractive host material with high loading potential.

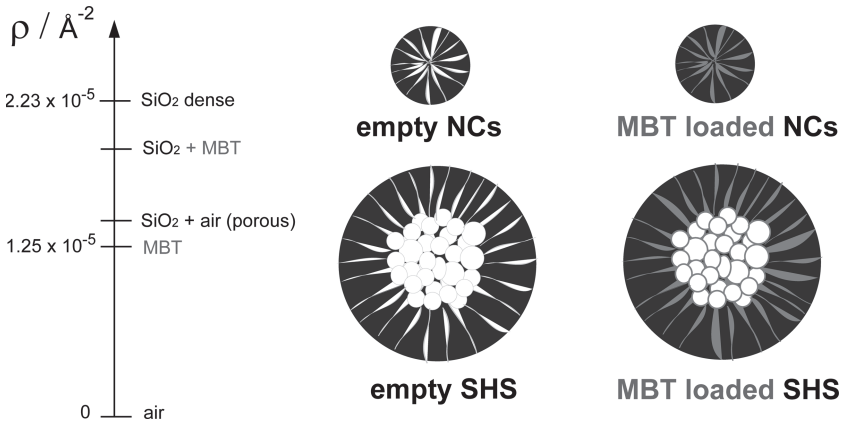

Figure 2. Scattering length densities (ρ_{sld}) of the materials present in the samples studied with SAXS and a graphical representation of the empty and MBT loaded silica containers.

2.2. Inhibitor Loading

The big pore volume and surface area of the synthesized silica containers suggest a high loading capacity. In addition, the complex pore system and container structural stability favours good inhibitor storage. A theoretical maximum loading capacity was calculated using the total pore volume of the empty NCs (≈1.2 mL g^{-1}) and SHS (≈0.8 mL g^{-1}) and the molar volume of MBT, V_m = 118 mL mol^{-1}. Assuming that only the mesopores are filled with MBT molecules with ρ_{MBT} = 1.42 g mL^{-1} a maximum loading capacity of 63 wt% for the NCs and 52 wt% for the SHS was determined.

The experimental MBT loading was quantitatively evaluated with TGA measurements (Supporting Information Figure S4). The decomposition temperature of MBT was previously determined to be ≈288 °C. Thus, the measured 20% weight loss around this temperature for both container types corresponds to the MBT loading, which indicates an equal amount of loaded inhibitor for both NCs and SHS. The experimentally determined MBT loading is less than half of the calculated maximum loading capacity of the containers and could be further increased by additional loading cycles. In order to decide, whether the loaded MBT is incorporated in the pores, N_2 sorption measurements of MBT@NCs and MBT@SHS dried powders were conducted (Supporting Information Figure S5). It was found that the incorporated MBT molecules cause a reduction in the total pore volume and surface area for both MBT@NCs and MBT@SHS. After an exact evaluation of the change in pore volume, a reduction factor of approximately two was determined after adsorption of the inhibitor molecules for both container types (Supporting Information Figure S5).

The difference in absolute scattering intensity of loaded and empty silica containers was investigated with SAXS in order to confirm the successful loading of the NCs and SHS pores with MBT. Since X-rays are scattered by electrons, the scattering strength depends on the composition of the investigated material. For this reason, the scattering length density ρ_{sld}, which is among others proportional to the electron density of the material, its molar mass and mass density, directly influence the scattering contrast. Therefore, the scattered intensity, which can be directly measured, relates to the Fourier transform of the scattering length density distribution in the sample.[23,24] **Figure 2** shows a comparison of the scattering length densities (ρ_{sld}) of the materials present in the studied samples. It is revealed that the addition of organic molecules or air to the silica reduces the scattering length density. For the NCs, the peak with a maximum at q ≈ 1.3 nm^{-1} can be attributed to the scattering of the mesopores (**Figure 3**a).[25] This peak is more intense for the empty NCs than for the MBT@NCs. In the case of empty NCs the scattering contrast is due to the difference between scattering length densities (ρ_{sld}) of silica (in the pore walls) and air (in the pores). A drop in scattering intensity for the mesopores can be caused by filling of the pores with the organic inhibitor MBT, which has a higher ρ_{sld} than air (Figure 2).[26] Thus, the smaller difference between ρ_{sld}(MBT) and ρ_{sld}(SiO_2 dense) causes a decrease in intensity in this q region. Small q values correspond to large scattering distances. Therefore, the detected scattering in the low q range is caused by the NCs. This is strongly influenced by

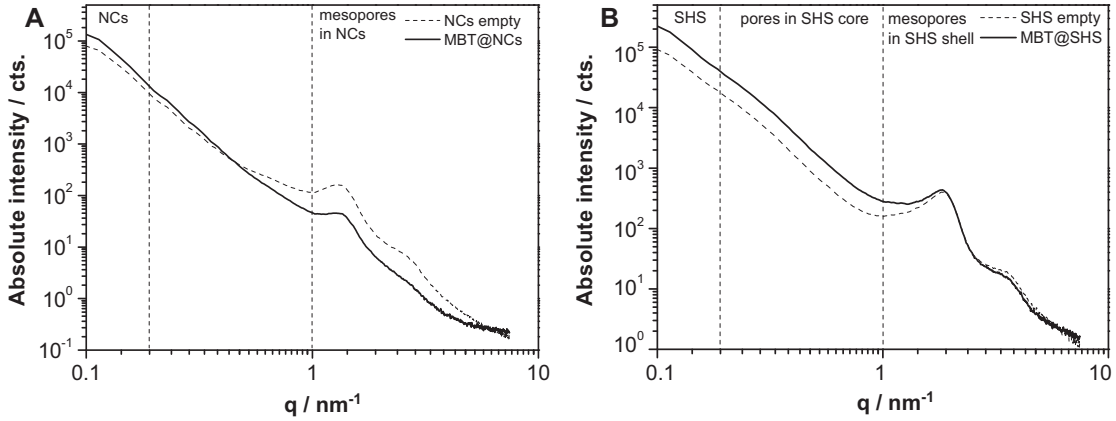

Figure 3. SAXS patterns of empty and MBT loaded a) NCs and b) SHS.

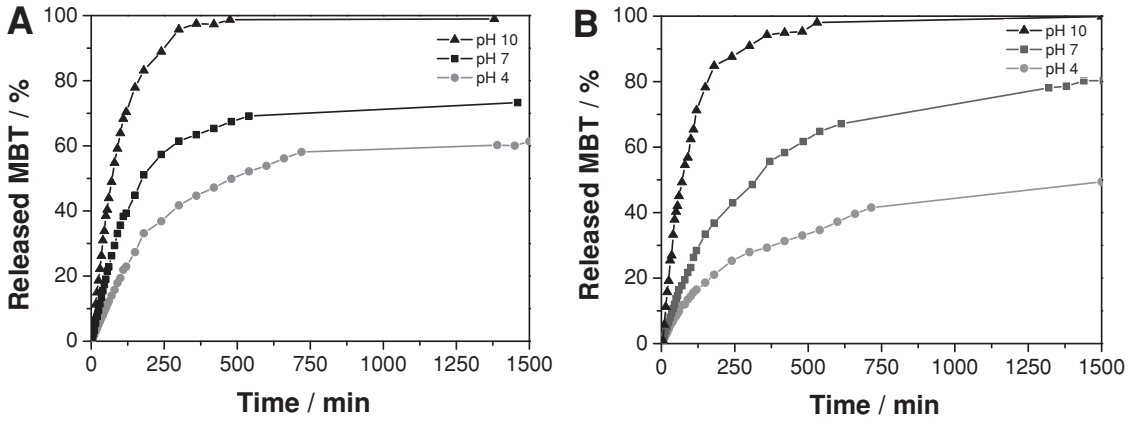

Figure 4. Profiles of release of MBT from a) MBT@NCs and b) MBT@SHS obtained during dialysis at different pH values and measured with UV-Vis spectroscopy.

the particle composition and its scattering contrast to the surrounding.[27,28] When the scattering of the NCs in contrast to the air between them is detected, the MBT loaded NCs have a higher scattering due to their higher ρ_{sld} compared to that of empty or air-filled NCs.

In the SAXS patterns of empty and MBT loaded SHS three regions, corresponding to different scattering distances are observed (Figure 3b). Starting from low q, these are caused by the scattering of i) the SHS particles, ii) the cage-like pores ($d_{pore} \approx$ 25 nm) in the SHS core, and (iii) the mesopores of the SHS shell.

Thus, the two peaks at $q > 1$ nm^{-1} probably correspond to the mesopores in the SHS shell and represent the scattering contrast between the silica matrix of the SHS shell and the pore interior of the mesopores in the SHS shell. For MBT loaded SHS, the scattering intensity is slightly lower than for empty SHS. This result is due to the weaker scattering contrast when the mesopores of the shell are filled with MBT compared to the case, when they are empty (i.e., filled with air). In the intermediate region of the SAXS patterns (0.2 nm^{-1}< q < 1 nm^{-1}), the scattering contrast reveals the difference between the ρ_{sld} values of the interior of the cage-like pores in the SHS core and the matrix (i.e., the SHS mesoporous shell) surrounding it. Accordingly, when the pores in the SHS core are empty and the mesopores in the SHS shell are filled with MBT, the difference between ρ_{sld}(air) and ρ_{sld}(SiO_2 + MBT) causes the scattering intensity. This was detected to be higher for MBT@SHS than for empty SHS because the ρ_{sld}(SiO_2 + air) is smaller than ρ_{sld}(SiO_2 + MBT). This result supports the assumption that the MBT is contained in the mesopores of the SHS shell. The scattering signal at q < 0.2 nm^{-1} represents the scattering contrast between SHS outer surface and air between the particles. Thus, the measured higher scattering intensity for MBT@SHS at low q indicates the presence of MBT adsorbed at the container outer surface and shell.

The results obtained from the combination of three analytical techniques (TGA, N_2 sorption and SAXS) suggest that the incorporation of MBT in the studied silica containers was successful. It is assumed that the highly concentrated inhibitor solution enters the particle pores without hindrance due to the small size of the inhibitor molecules (<1 nm), which is less than 1/3 of the diameter of the silica container pores. It should be noted that the silica containers presented in this work possess much better encapsulating and storage properties than previously reported similar containers. This makes the studied containers applicable wherever high uptake and controlled delivery of encapsulated molecules are required.

2.3. Inhibitor Release

The release of the MBT from the MBT@NCs and MBT@SHS was determined using a dialysis technique at pH = 4, 7 and 10. The chosen acidic and basic pH values are typically achieved during the corrosion of aluminium alloys and can be utilized as triggers for inhibitor release. The amount of released MBT was monitored with UV-Vis spectrometry for 24 h. The profiles obtained at different pH values are similar in shape for both MBT@NCs and MBT@SHS and reveal two stages of inhibitor release (**Figure 4**). An initial fast release is followed by a more gradual release. In the first stage a high amount of MBT is released within the first hours. This initial burst release is pH-dependent and particularly important as it describes the amount of inhibitor available on contact with a corrosive area. The MBT release in alkaline conditions for both container types is faster than for acidic and neutral conditions. In addition, the amount of released MBT is the largest at pH 10. As corroding AA2024-T3 areas have high basicity at the cathode, the larger release at pH = 10 is desirable. On the other hand, the reduced release at pH = 7 should limit the leaching of inhibitor from the coating. The second stage of the release profiles is characterized by a gradual MBT release reaching a saturation level. From the comparison of the results for MBT@NCs and MBT@SHS, it is evident that the MBT release from the SHS is slower. This can be due to the longer mesopores in the SHS shell (≈100 nm) compared to the ones of NCs (≈40 nm), providing more interaction sites between MBT molecules and pores walls. A prolonged release is of great advantage for long-term corrosion inhibition. The stabilization of MBT release for longer immersion times can be due to reaching a maximum MBT solubility in the release medium and/or MBT degradation to sub-products (e.g., 2-hydroxybenzothiazole, benzothiazole).[29] The maximum released amount of MBT differs with pH because of the pH dependent solubility of MBT.[30,31] Thus,

the release study revealed a stimuli-responsive (pH dependent) MBT release from both silica containers.

2.4. Physical Properties of the Coating

The water-based epoxy coating used as a passive coating matrix in this study is a two-component model coating established as a primer for aerospace applications. Single layer organic coatings were applied on aluminium alloy AA2024-T3 plates using a spiral bar coater for 50 µm wet coating thickness. Prior to application, water suspensions of MBT@NCs or MBT@SHS of different concentrations were prepared and added to the pre-mixed two-component coating matrix. The following container fractions with respect to the cured coatings were embedded: 0.04, 0.2, 0.5, 0.7 and 1.7 wt%. The thickness of the cured coatings deposited on the aluminium alloy was measured with a coating thickness gauge using the Eddy-current principle.[32] Similar coating thicknesses ≈20 µm were obtained for both coating systems (Supporting Information Figure S6). A measurement error of ≈20% was obtained due to the high metal surface roughness and the manual coating application method. Considering the measurement conditions, no strong influence of the container size on the coating thickness could be observed, and the thicknesses of both coating systems are similar. The results from the adhesion test with freshly cured organic coatings are shown in Supporting Information Figure S7. A measurement error of 10% was considered due to a glue failure, which led to an incomplete removal of the tested coating area. No exact dependence between measured adhesion, container size and concentration could be observed. All organic coating formulations exhibit similar adhesion to the metal substrate, ≈3.5 MPa.

2.5. Anticorrosive Properties of the Coating

2.5.1. Active Corrosion Resistance

The influence of the container size on the self-healing ability of the anticorrosive coatings was evaluated using SVET. The organic coatings containing different concentrations of MBT@NCs or MBT@SHS were scratched in a controlled way to expose the underlying metal to the corrosive environment (0.1 M NaCl) and to induce corrosion. The introduced scratches were ≈3 mm long, ≈20 µm wide and ≈60 µm deep. The scratch dimensions and the dense distribution of intermetallic particles (IMPs) in the aluminium alloy (≈300 000 particles/cm^2) suggest the exposure of enough IMPs to 0.1 M NaCl to trigger localized corrosion.[33] These IMPs can act as anodes or cathodes depending on their composition, distribution and corrosion stage.[34] Generally, Cu-rich IMPs act as cathodes compared to the surrounding aluminium matrix (the anode) due to their more noble character. The electrochemical reactions occurring at the anode and cathode induce a positive anodic and a negative cathodic current flow, which lead to potential differences in the electrolyte solution. With SVET, the vibrating measuring electrode was moved above the scratched sample and the potential differences were detected, which were then converted into an electrical current density over the scanned area. In the further data analysis, the current density maps taken periodically were integrated to calculate the minimum (cathodic) and maximum (anodic) currents as a function of time.[35,36] With SVET only currents for anodes and cathodes with sufficient distance between each other could be detected. This limitation comes from the large coating thickness (≈20 µm), big measuring height (300 µm), and the assumption that the current between anode and cathode flows in a hemisphere.

It is suggested, that the self-healing effect observed with the studied coatings is triggered by the onset of corrosion and the consequent pH increase (pH ≈ 10) above the cathodes built in AA2024-T3. Basic pH favours the release of the loaded MBT, which forms a protective layer on the attacked metal surface. The suggested self-healing mechanism is observed in the SVET data by an increase in the anodic current accounting for the initiation of corrosion and the consequent suppression of the anodic current revealing the corrosion inhibition.

The detected anodic currents as a function of time for the samples coated with organic coatings containing different concentrations of MBT@NCs are shown in **Figure 5**. A constant increase in anodic current with time reflects the dissolution of aluminium due to ongoing corrosion. Such a behavior was

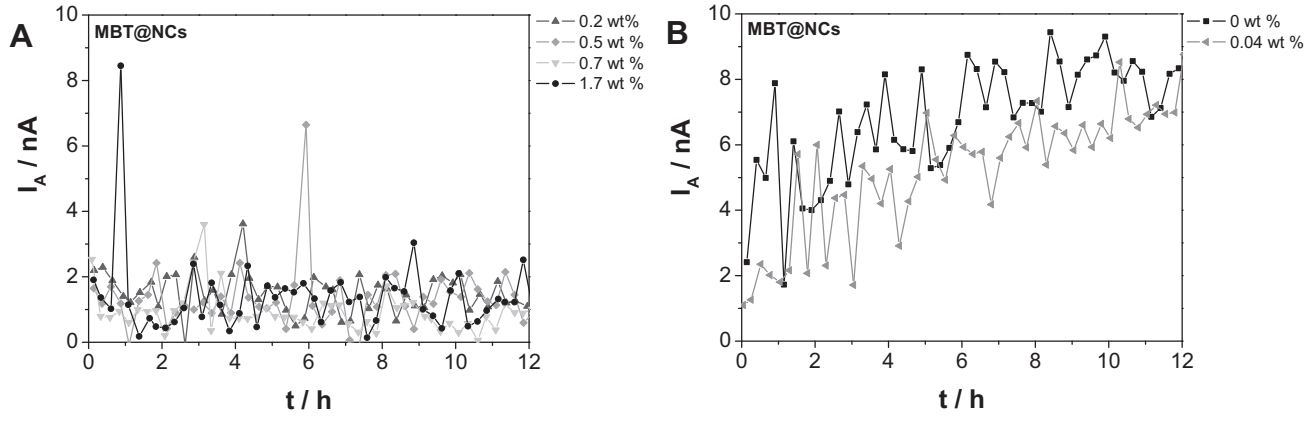

Figure 5. Maximum anodic currents detected with SVET over the scanned scratched area during a 12 h immersion period in 0.1 M NaCl. Results are shown for samples coated with an organic coating containing different MBT@NC concentrations demonstrating a) efficient and b) unsatisfactory active corrosion inhibition.

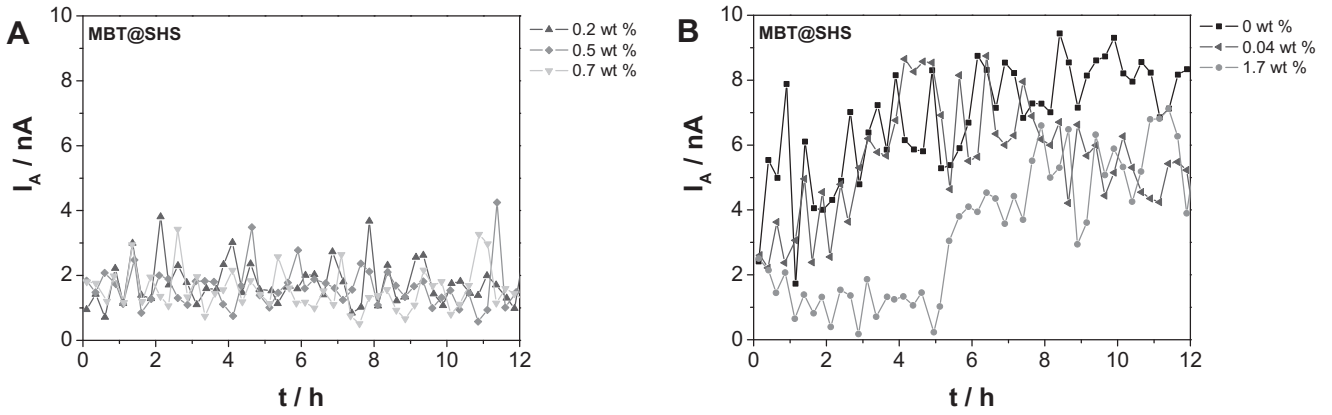

Figure 6. Maximum anodic currents detected with SVET over the scanned scratched area during a 12 h immersion period in 0.1 M NaCl. Results are shown for samples coated with an organic coating containing different MBT@SHS concentrations demonstrating a) efficient and b) unsatisfactory active corrosion inhibition.

detected for samples with too low inhibitor amount (c(MBT@NCs) = 0.04 wt%), which was not enough to actively suppress corrosion (Figure 5b). By increasing the amount of available inhibitor in the coatings (c(MBT@NCs) ≥ 0.2 wt%), better active corrosion resistance and self-healing ability were observed. This is revealed by the suppression of the measured anodic current to values lower than ≈2 nA. Even very high amount of embedded NCs (1.7 wt%) leads to good corrosion resistance. This suggests for the studied concentration range (c(MBT@NCs) = 0.04–1.7 wt%), that the coating barrier properties and integrity are preserved, when high amount of small containers is embedded. In contrast, embedding bigger containers at the same high concentration (c(MBT@SHS) = 1.7 wt%) led to worse barrier properties and insufficient active corrosion resistance (**Figure 6**b). For the first 5 h of immersion in 0.1 M NaCl, this sample managed to inhibit successfully corrosion due to the high amount of available inhibitor. However, after 5 h the deterioration of coating barrier properties dominated the overall anticorrosion performance and led to failure in corrosion inhibition.

When MBT@SHS are embedded at intermediate concentrations (0.2–0.7 wt%), the same behavior as for the MBT@NCs was observed (Figure 6a). However, no distinct increase of I_A, which would reveal the onset of corrosion, was observed for the samples with MBT@SHS. The apparent active corrosion inhibition could be caused by corrosion reactions taking place between cathodes and anodes in close proximity. Thus, the resulting corrosion current develops very close to the metal surface and cannot be detected by the measuring electrode at 300 µm above the coating surface.

Generally, the currents detected with SVET for samples coated with organic coatings are very low. This is due to their good self-healing ability combined with good adhesion and coating barrier properties.

In order to confirm the results obtained with SVET, the coated samples and the area around the scratch were investigated with SEM after the SVET study (after 12 h immersion in 0.1 M NaCl).

The extent of corrosion was assessed in accordance with the amount of corrosion products formed around the scratched area (Supporting Information Figure S8,S9). For the control sample, a big amount of corrosion products is accumulated at two sites along the scratch, suggesting one anode site between those. In addition, the coating damage at the borders of the scratch reveals a deterioration of the coating barrier properties due to corrosion. Similar SEM results were obtained for the coatings containing a small concentration of MBT@NCs or MBT@SHS (0.04 wt%). Thus, the big amount of corrosion products around the scratch confirms an insufficient active corrosion resistance for low inhibitor amount, as detected with SVET. In contrast, the coatings with efficient active corrosion resistance (0.2–0.7 wt%) are characterized by smooth surfaces and very little accumulation of corrosion products. The corrosion for these samples was inhibited successfully and only a small amount of corrosion products could be detected by SEM. These were detected as i) fine grains dispersed in a thin layer on the coating surface and/or ii) accumulation of small amount of corrosion products in the scratch.

The presence of corrosion products, even a small amount, confirms that the corrosion process was initiated. Thus, when sufficient amount of inhibitor was available in the coating, it was released upon corrosion onset to inhibit the metal dissolution and the further formation of corrosion products. However, this is valid only, when also the barrier properties of the coatings are preserved. The high amount of available inhibitor could not compensate for the deteriorated barrier properties on long term, as revealed by SVET and SEM data for the sample with 1.7 wt% MBT@SHS (Supporting Information Figure S9).

2.5.1. Passive Corrosion Resistance

Coating barrier properties are an important aspect of the overall coating performance. In order to investigate the long-term protection provided by the developed coatings, coated AA2024-T3 aluminium alloy plates were immersed in 1 M NaCl, and their passive corrosion resistance was studied with electrochemical impedance spectroscopy (EIS) over a time range of 30 days. This long immersion time was chosen due to the large thickness of the studied coatings, which are usually applied as primers and should exhibit superior barrier properties.

The impedance spectra of the AA2024-T3 coated with organic coatings containing different MBT@NC or MBT@SHS

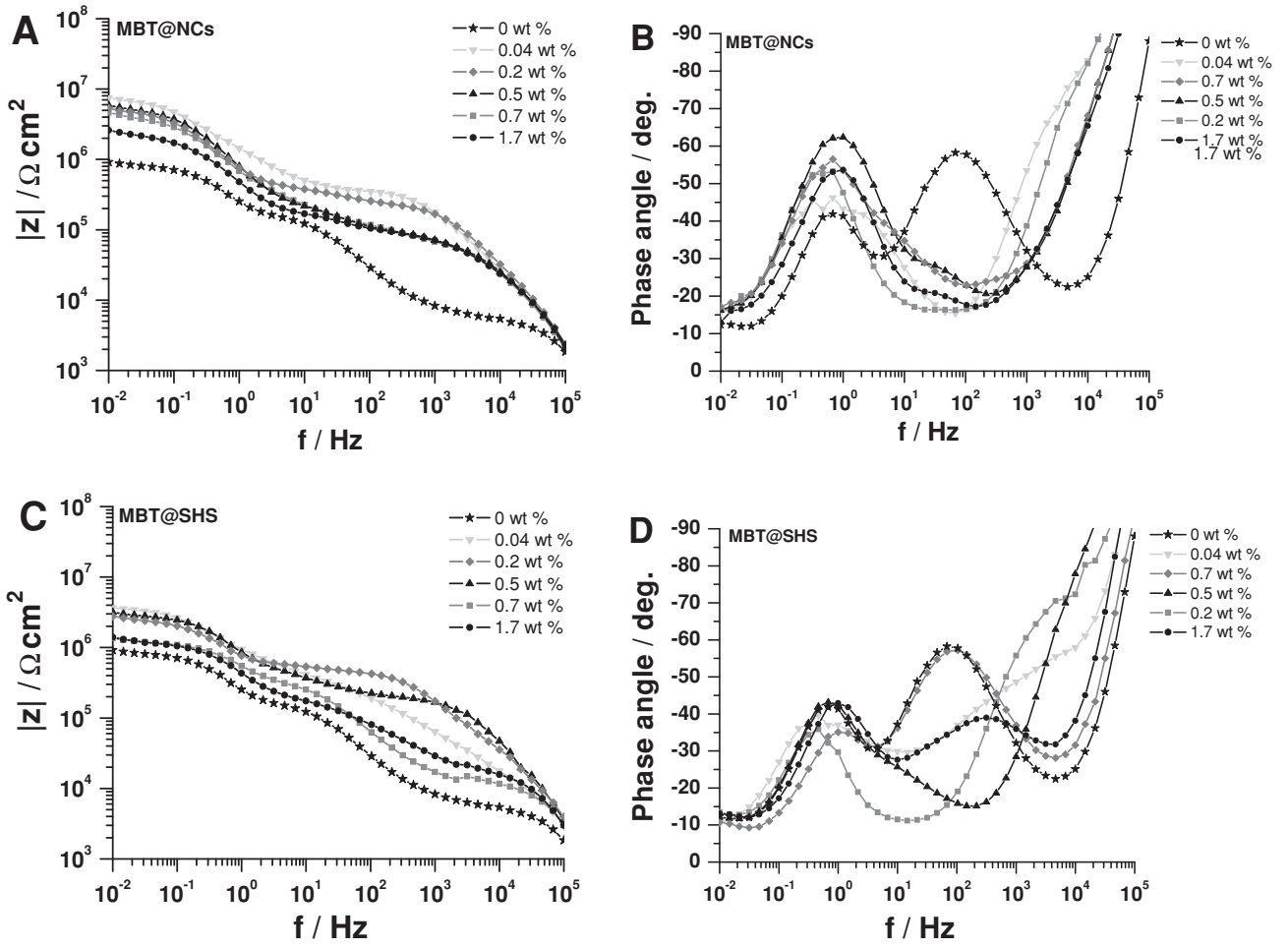

Figure 7. Bode plots showing the absolute impedance (a,c) and phase angle (b,d) as a function of frequency after 30 days immersion in 1 M NaCl of AA2024-T3 substrates coated with organic coatings containing different concentrations of MBT@NCs (a,b) and MBT@SHS (c,d).

concentrations after 30 days immersion in 1 M NaCl are represented in the form of Bode plots in **Figure 7**. The spectra can be generally divided into three frequency regions (high, intermediate and low f), which correspond to different parts of the coated samples. The electrochemical response of the coating is represented at high frequencies. Relaxation processes occurring closer to the metal surface are revealed in the EIS spectra at lower frequencies. These can be associated with the native aluminium oxide layer between coating and metal surface (intermediate frequencies, C_{oxide} and R_{oxide}) and the occurrence of corrosion (low frequencies, C_{dl} and R_{ct}). After a long immersion time (30 days), the oxide layer is deteriorated and its electrochemical response suppressed. Thus, the corrosion process (C_{dl} and R_{ct}) and mass transport (C_w and R_w) of corrosive species dominate the EIS spectra at lower frequencies (1–0.01 Hz).[8]

The impedance measured at the lowest frequency ($|Z|_{0.01Hz}$) reflects the corrosion resistance of the coatings (**Figure 8**a). The comparison of the values of $|Z|_{0.01Hz}$ obtained after 30 days immersion in 1 M NaCl for the coating systems containing MBT@NCs or MBT@SHS reveals two dependencies. First, bigger size of embedded containers leads to worse passive corrosion resistance. Second, higher concentrations of embedded containers deteriorate the coating barrier properties. In order to better understand the resistive and capacitive contributions of each part of the coating systems, the EIS spectra obtained after 30 days immersion in 1 M NaCl (Figure 7) were fitted using the equivalent circuit shown in Figure 8b. This equivalent circuit was chosen because of its reasonable physical meaning and fit quality ($\chi^2 \approx 0.01$). It describes very well the electrochemical response of the relaxation processes occurring in the coated samples after this long immersion time (30 days).

The obtained fitting parameters for the coating response (R_{coat} and C_{coat}) and occurrence of corrosion (R_{ct} and C_{dl}) reflect the corrosion resistance of the studied coating systems and are presented in **Figure 9**. The coating resistance reflects the presence of pores and cracks in the coating. High R_{coat} values correspond to better barrier properties, which can be due to fewer defects in the coating and/or less area of delaminated coating. The resistance of the coating without containers is almost one order of magnitude lower than for the ones with containers (Figure 9a). This reveals that the unmodified coating is more degraded compared to the modified coatings, which is likely

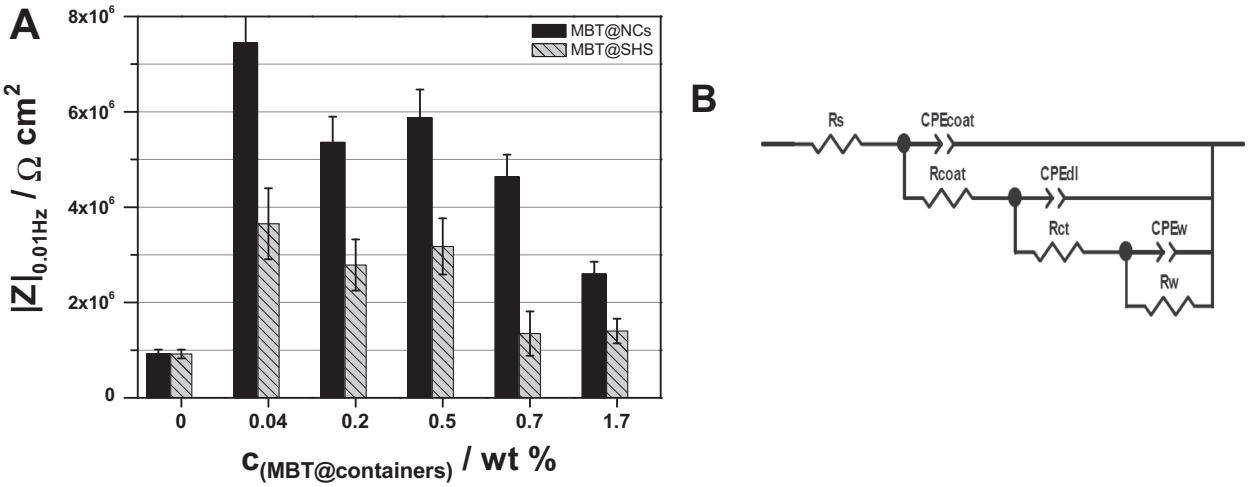

Figure 8. a) Impedance |*Z*| measured at 0.01 Hz after 30 days immersion in 1 M NaCl for organic coatings with different concentrations of MBT@NCs or MBT@SHS and b) the equivalent circuit used to fit the EIS spectra obtained after 30 days immersion in 1 M NaCl.

to be due to the absence of active protection. Incorporating inhibitor loaded containers in the coating provides self-healing functionality but can also deteriorate the integrity of the coating matrix. The latter, negative effect was more pronounced for the big MBT@SHS as revealed by the lower R_{coat} values in comparison to the R_{coat} values for MBT@NCs. This might be due to the limited adjustment of the polymer coating to bigger silica containers. This limited coating flexibility leads to the formation of more imperfect sites and diffusion pathways for the aggressive electrolyte. When high amount of containers is

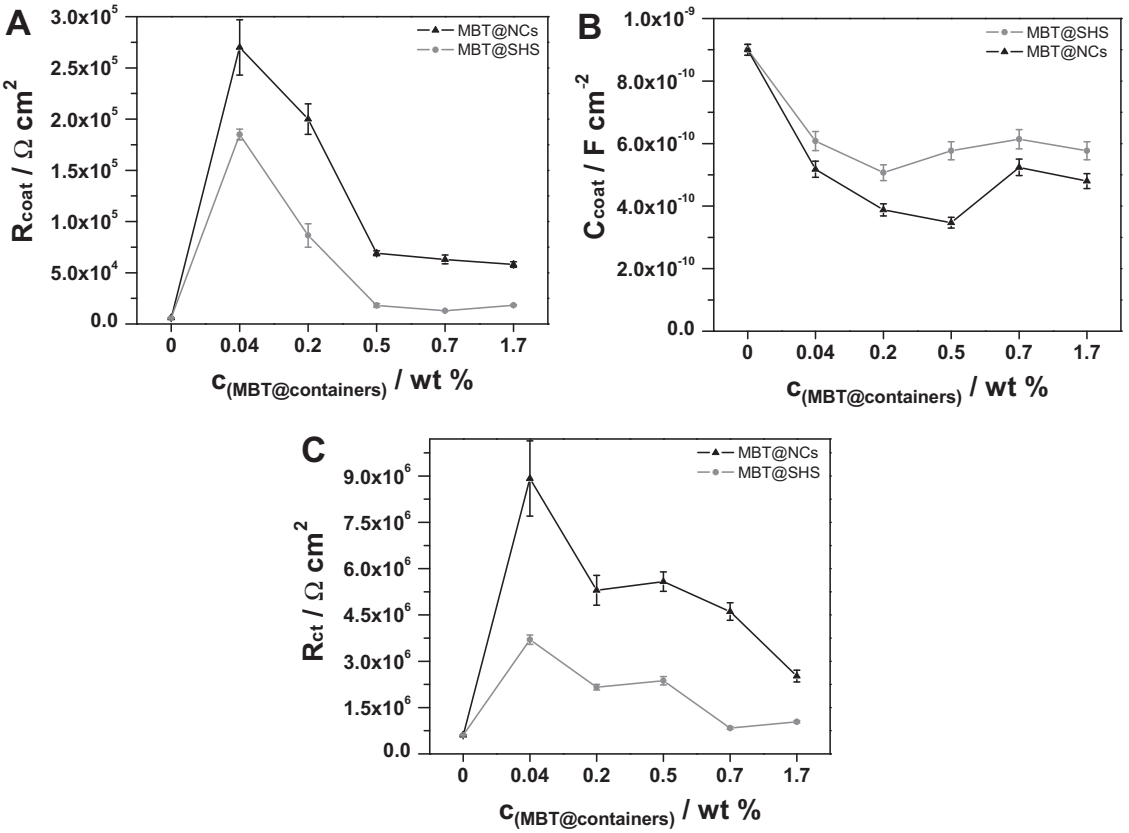

Figure 9. Calculated data for the a) coating resistance (R_{coat}), b) coating capacitance (C_{coat}), c) charge transfer resistance (R_{ct}), and d) double layer capacitance (C_{dl}) obtained by fitting of the EIS spectra using the equivalent circuit shown in Figure 8b. EIS spectra obtained for the coating systems with MBT@NCs or MBT@SHS after 30 days immersion in 1 M NaCl were fitted.

embedded, the coatings with the smaller MBT@NCs exhibit again better barrier properties compared to the ones with MBT@SHS. This suggests a low agglomeration tendency of the MBT@NCs due to their possibly better dispersibility in the wet coating formulation and/or stronger adhesion to the dry coating matrix.

The three time constants observed in the Bode plots (Figure 7b,d) correspond to phase angles that deviate from −90 °. Considering this deviation, constant phase elements (CPE) instead of capacitances were used for the fitting. The capacitance values were calculated using Equation 1.

$$C = Q(\omega_{max})^{n-1} \quad (1)$$

In Equation 1, Q and $0 < n \leq 1$ are parameters calculated for the CPE by fitting and ω_{max} is the radial frequency at which Z'' reaches a maximum for the respective time constant.[37]

The capacitance of the coating (C_{coat}) is sensitive to the water permittivity of the coating. Its dependence can be described by the simple model of a dielectric, with a capacitance C that is directly proportional to the relative dielectric constant of the coating and to the area A of the capacitor (in this case the surface area of the coating), and inversely proportional to the coating thickness d:

$$C = \frac{\varepsilon \varepsilon_0 A}{d} \quad (2)$$

The constant ε_0 represents the dielectric constant of free space, (8.854×10^{-14} F cm^{-1}). The dielectric constant (ε) of polymers is typically in the range 3–8 and of water is 78.3 at 25 °C and the effective dielectric constant is given as a weighted average of the water and polymer volume fractions.[38] Accordingly the penetration of water in the organic coating should lead to a rise in the mixed dielectric constant, resulting in a higher capacitance. Assuming a coating thickness of 20 µm (the average thickness of the studied coatings), A of 1 cm^2 and a dielectric constant of 8 for an organic coating with no water content, a capacitance value of 3.5×10^{-10} F cm^{-2} is calculated. The obtained C_{coat} value of $\approx 9 \times 10^{-10}$ F cm^{-2} for the bare coating is approximately 2.5 times higher and indicates water penetration from the electrolyte into the coating during the 30 days exposure time (Figure 9b). The coatings with MBT@NCs exhibit lower C_{coat} for all concentrations compared to the ones with MBT@SHS. This suggests a higher water uptake for coatings containing the bigger MBT@SHS, which can be due to the higher extent of diffusion pathways and defects in these coatings. The results for the coating capacitance are in agreement with the resistive response of the coating. This confirms that increasing the size and concentration of embedded containers deteriorates the coating barrier properties.

The corrosion rate is described by the charge transfer resistance (R_{ct}). R_{ct} reflects the kinetics of the electrochemical reactions at the interface and is directly dependent on the active corrosion inhibition. Accordingly, the higher R_{ct} values for modified coatings can be due to the embedded inhibitor and the self-healing effect (Figure 9c). The incorporation of high amount of MBT loaded containers in the coatings compromises the coating barrier properties, as described above. This barrier effect influences the extent of corrosion and is reflected in the obtained results for R_{ct}. Thus, the lower R_{ct} values for coatings with MBT@SHS can be explained by the worse barrier properties of the coating.

The double layer capacitance (C_{dl}) is directly related to the metal area exposed to the electrolyte. This area results from defects in the coating and increases with higher degree of coating degradation. It also provides information about the wet adhesion of the coating to the metal. Accordingly, the high C_{dl} values for the unmodified coating are due to the high extent of damage and defects in the coating (Figure 9d). For modified coatings, the lower values of C_{dl} compared to the unmodified one can be attributed to the suppressed corrosion evolution due to the self-healing ability of the coatings. The higher C_{dl} values for bigger container size and amount account for higher extent of corrosion. This can be induced by the higher degree of coating degradation or worse adhesion of the coating to the metal surface. Thus, the obtained results for C_{dl} are in agreement with the resistive response (R_{ct}) of the studied samples. Overall, the EIS study confirmed the better anticorrosion performance of the coating systems with MBT@NCs and MBT@SHS compared to the unmodified, bare organic coating. Despite the loss of barrier efficiency observed for high amount or bigger embedded containers, an enhanced long-term corrosion resistance was provided due to the self-healing functionality of the modified coatings.

In order to better understand the effect of embedded containers on the coating barrier properties, the contribution of active corrosion resistance needs to be excluded. Therefore, only empty containers were embedded in the organic coating. Their concentration corresponds to the container concentration in 0.5 wt% MBT@NCs and MBT@SHS. This was chosen due to the optimum overall anticorrosion performance of both coating systems containing 0.5 wt% MBT loaded containers. Additionally, MBT was incorporated directly into the organic coating to study its impact on the passive corrosion resistance. The MBT concentration is 0.1 wt% and equals the amount of MBT in 0.5 wt% MBT loaded containers, considering the MBT loading detected with TGA (20 wt%). The EIS spectra of the samples with these coatings after 30 days immersion in 1 M NaCl are shown in **Figure 10**. Lower $|Z|$ values for all frequency regions were detected for the samples with empty containers as compared to the corresponding coatings with MBT loaded containers. This is possibly due to the absent functionality of the coatings to actively inhibit corrosion and improve the long-term corrosion resistance. It is important to note that the direct incorporation of MBT in the organic coating led to the worst electrochemical response, classifying this coating formulation as inefficient to inhibit corrosion on long-term.

In order to better understand the processes and their contributions to the overall electrochemical response of the studied systems, the EIS spectra shown in Figure 10 were fitted using the equivalent circuit shown in Figure 8b.

The resistive responses of the coating (R_{coat}) and charge transfer processes (R_{ct}) were shown because these describe directly the barrier properties and extent of coating degradation (Figure 10c). The low R_{coat} value for the coating modified with MBT suggests a detrimental effect of MBT on the coating matrix, when directly introduced into the coating. Additionally, the low R_{ct} accounts for a possible deactivation of the inhibitor, which could explain the insufficient active corrosion inhibition.

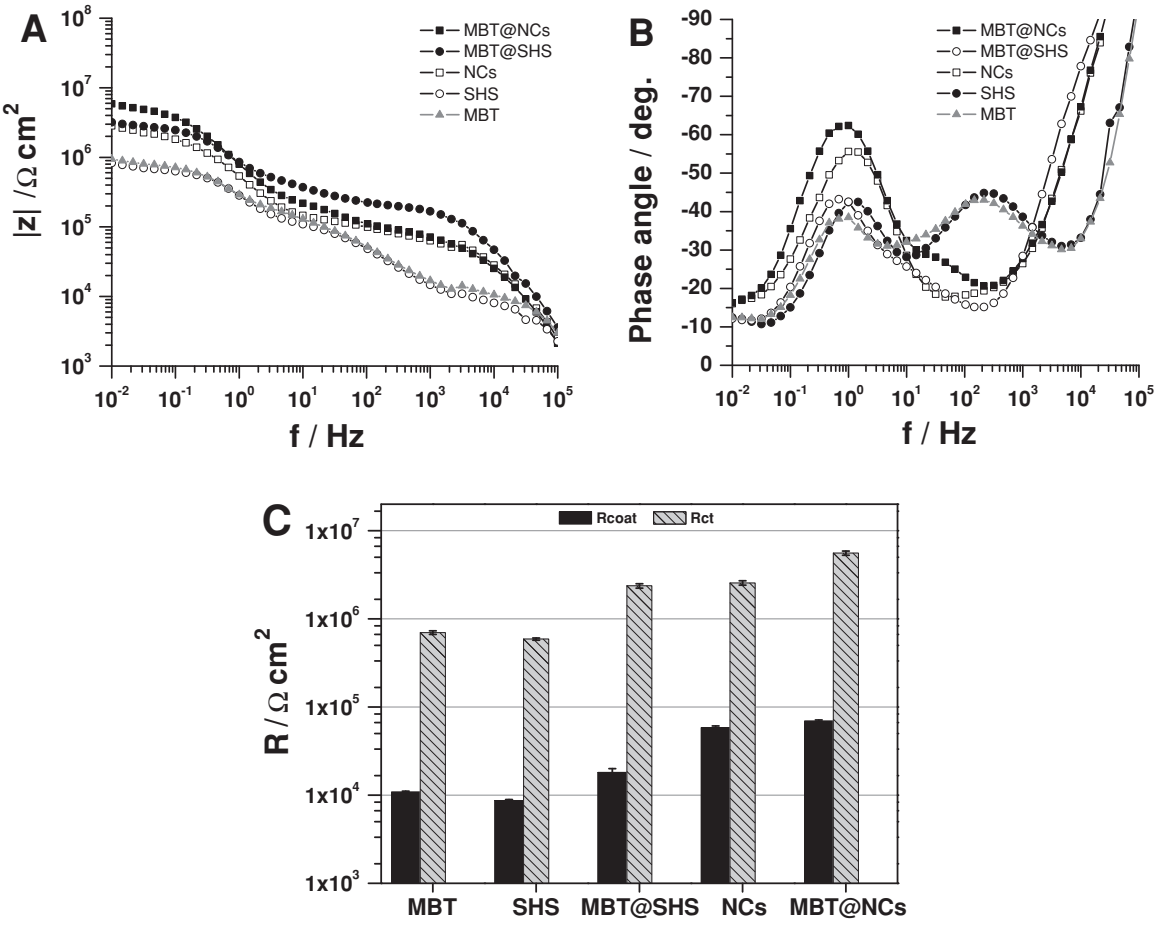

Figure 10. Bode plots showing the a) absolute impedance and b) phase angle as a function of frequency after 30 days immersion in 1 M NaCl of AA2024-T3 substrates coated with organic coatings doped with MBT, empty and MBT loaded silica containers (NCs or SHS), c) parameters (R_{coat} and R_{ct}) obtained by fitting of the EIS spectra using the equivalent circuit in Figure 8b.

Conversely, these negative effects are not observed, when the MBT does not come into a prolonged physical contact with the coating matrix. Therefore, the presence of encapsulated MBT in the coating improves the coating corrosion resistance. The R_{coat} values obtained for coatings doped with empty NCs are almost one order of magnitude higher than those for coatings with SHS. The same trend is observed also for the R_{ct} values with a difference of a factor of five. This indicates an adverse effect of bigger containers on the coating barrier properties. This can be attributed to the higher stress introduced in the organic coating matrix by bigger, embedded containers, leading to more cracks and defects. In addition, a possible poorer distribution of SHS in the coating would lead to the formation of agglomerates, which are bigger than the ones of NCs, considering the almost ten times bigger size of the SHS.

A Machu test of the coated samples with a cross-cut (3×3 cm^2 and 1 mm thick) was performed for visualization of the corrosion protection performance and self-healing ability of the coating. The samples were exposed to an aggressive, oxidative mixture (5% NaCl, 1% CH_3COOH and 0.15% H_2O_2) with pH ≈ 3 for 48 h.[39] This method provides a criterion for the evaluation of the extent of corrosion underneath a coating and its effect on adhesion. The length of the lateral damage underneath the coating serves as a measure of anticorrosion efficiency. The result of the Machu test is considered satisfactory when no infiltration exceeding 0.5 mm on both sides of the scratch is observed. Samples fulfilling this requirement can obtain the QUALICOAT quality label. In order to evaluate the infiltration, the area with the cross-cut was scratched after the test and photographs were taken (**Figure 11**).

The samples coated with unmodified organic coating (the control sample) providing only passive protection, revealed unsatisfactory performance and the infiltration was ≈5 mm on both sides of the scratch. The organic coatings with directly introduced MBT or empty containers (NCs and SHS) performed the worst of all studied samples, as revealed by the almost complete coating delamination around the scratched area. This indicates bad corrosion inhibition and poor adhesion of coating to metal.

Surprisingly, also for the coatings with MBT@SHS big infiltration was observed. The corrosion attack for low c(MBT@SHS) was so extensive that the coating could be easily peeled off. This is possibly due to insufficient amount of inhibitor and poor adhesion. Coatings with high c(MBT@SHS) suppressed

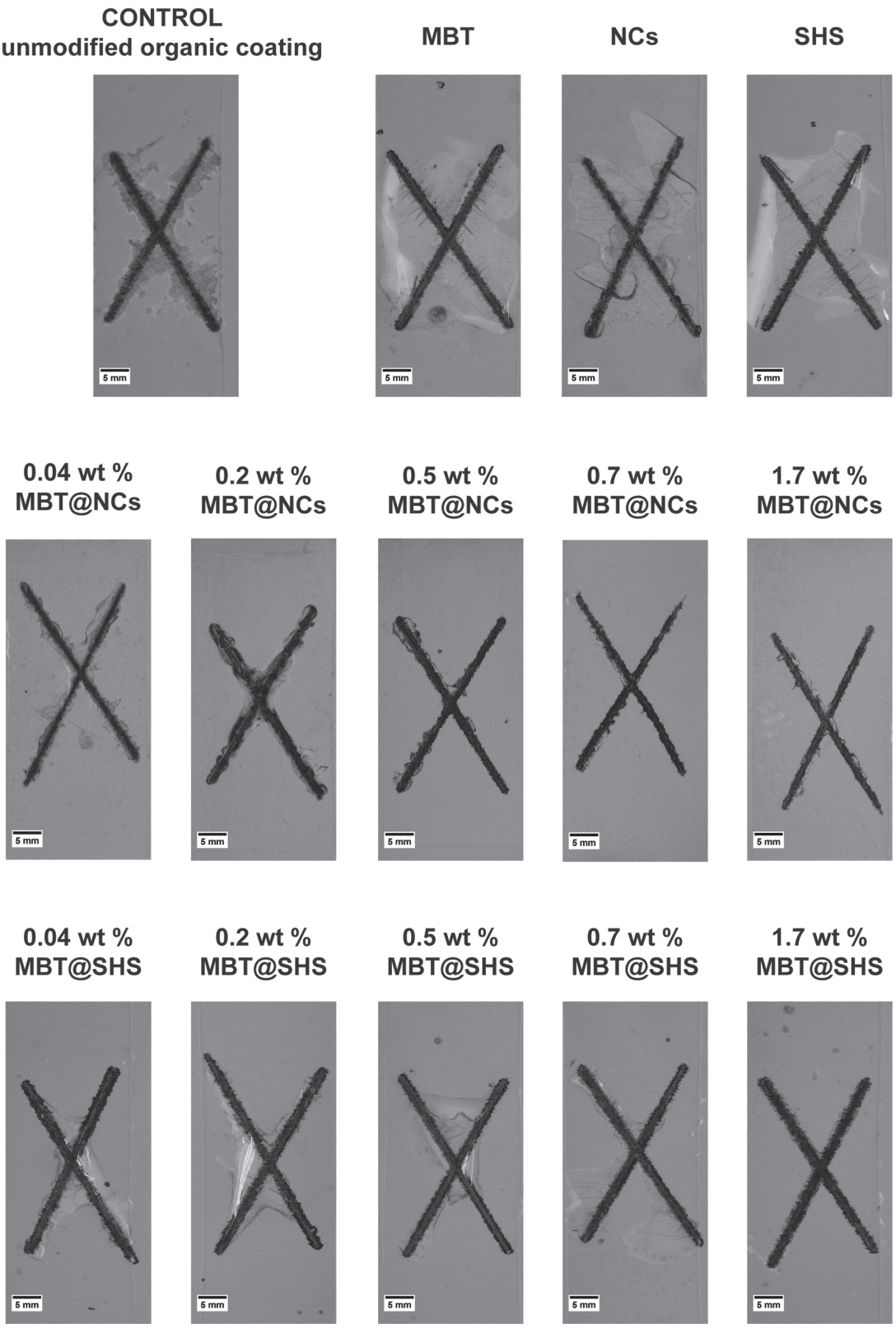

Figure 11. Photographs of the coated samples tested with the Machu test for 48 h at 37 °C in an aq. mixture of 5% NaCl, 1% CH_3COOH and 0.15% H_2O_2.

the corrosion evolution more successfully but the infiltration was still above the required value of 0.5 mm. The failure for these can be explained by their poor barrier properties, as indicated by the dark spots revealing localized corrosion attack on the unscratched area.

Better Machu test results were obtained for the samples coated with organic coatings containing MBT@NCs. This is probably due to their self-healing functionality and better barrier properties compared to the coatings with MBT@SHS. In addition, the Machu test results suggest the good wet adhesion of the coatings with MBT@NCs to the metal substrate. The incorporation of MBT at sufficiently high amount (c(MBT@NCs) > 0.5 wt%) leads to satisfactory overall anticorrosion performance of these coatings in the Machu test. The infiltration was measured to be below 0.5 mm on both sides of the scratch, classifying the coating systems with 0.7 wt% and 1.7 wt% MBT@NCs for the QUALICOAT quality label.

3. Conclusions

In order to qualify an anticorrosion coating with embedded containers and feedback activity, it is not sufficient to consider only the anticorrosion activity but also the barrier function, the adhesion and mechanical strength of the coating. Therefore one of the important factors influencing the performance of active anticorrosive coatings based on embedded containers is the container size. In this paper, mesoporous silica containers with similar inhibitor storage capacity but different sizes ($d_1 \approx 80$ nm and $d_2 \approx 700$ nm) were embedded at different concentrations in 20 µm thick water-borne epoxy coatings. The obtained coating systems exhibited similar physical properties (thickness and dry adhesion) for both container types over the whole concentration range. The similar amount of loaded inhibitor (20 wt%) in both container types was a prerequisite for comparable active corrosion inhibition. The results of the scanning vibrating electrode technique (SVET) revealed worse self-healing performance for the coatings impregnated with bigger containers. This effect was very strongly pronounced when high amount of containers (1.7 wt%) was embedded. The container size had a significant impact on the coating barrier properties, as shown using electrochemical impedance spectroscopy (EIS). It was found that embedding bigger containers leads to doubled reduction of coating barrier properties. Bigger containers introduce more strain and defects in the organic coating matrix due to their size and large agglomerates.

In spite of the decrease in barrier effect, observed with inclusion of containers of bigger size or amount, a better long-term anticorrosion performance of all coatings modified with nanocontainers of both types as compared to the unmodified one was observed. This is due to the self-healing effect provided by the inhibitor (2-mercaptobenzothiazole) encapsulated in the nanocontainers.

4. Experimental Section

Materials: All chemicals used were commercially available and used without further purification. Tetraethyl orthosilicate (TEOS, ≥99%), cetyltrimethylammonium chloride (CTACl, 25% in H_2O), cetyltrimethylammonium bromide (CTAB) and triethanolamine (TEA) were purchased from Sigma-Aldrich. Hydrochloric acid (HCl, 37%) was supplied by Carl Roth. Sodium chloride (NaCl, analytical grade), sodium hydroxide (NaOH, 1 M), acetic acid (100%) and 2-mercaptobenzothiazole (MBT) were obtained from Merck. Ethanol (EtOH) was purchased from VWR Prolabo. Hydrogen peroxide (H_2O_2, 30%) and buffer solutions were supplied by Fluka. Dialysis tubing (Spectra/Por 6, 50 kDa MWCO) was obtained from Spectrum. The water used in all experiments was purified in a three-stage Millipore Milli-Q Plus 185 purification system. The aluminium alloy, AA2024-T3, used for corrosion testing was supplied by EADS Deutschland and cut into appropriate dimensions for the different analyses of the anticorrosive properties. The water-based organic coating was provided by Mankiewicz GmbH. For adhesion tests, 3M two component adhesive (Scotch-Weld DP 490) was used.

Synthesis Containers: Two types of mesoporous silica containers of different size were synthesized and studied in this work. The first type is mesoporous silica nanocontainers (NCs), which were synthesized applying the procedure described previously.[40] Briefly, a mixture of TEOS/CTACl/TEA/H_2O/EtOH in a molar ratio of 1:0.27:1:137:6 was stirred for 2 h at 80 °C. The template was extracted in a HCl/ethanol mixture for 30 min under ultrasonic agitation. After several centrifugation and washing steps, the NCs free of template were dried in air at 60 °C overnight. The second type of containers is spherical hollow silica particles (SHS) with porous shell and submicron size (≈700 nm). SHS were synthesized following a sol-gel/emulsion (oil-in-water/ethanol) approach suggested by Teng et al.[41] First, a 40.5 mL mixture of water and ethanol in a volume ratio of 0.59 (15 mL ethanol/ 25.5 mL water) was prepared. To this mixture 0.5 mL of TEOS and 0.08 g of CTAB were added. This was followed by addition of 0.5 mL ammonia solution (25 wt% NH_3 in water) under stirring (700 rpm). The reaction mixture was stirred at this speed at room temperature for 3 h. The white precipitate was then separated by filtration, washed with water and dried at 70 °C overnight. The surfactant molecules were removed by calcination of the dried powder in air at 550 °C for 5 h.

Loading of the silica containers was conducted in a second step after their synthesis. The synthesized containers were mixed with an acetone solution of 2-mercaptobenzothiazole, MBT (80 mg mL^{-1}) and stirred for 4 h. The loaded containers (MBT@NCs or MBT@SHS) were separated by centrifugation, washed with water to remove excess of MBT on the container surface and dried overnight at 60 °C.

The MBT release from the loaded silica containers was determined using a dialysis technique in buffer solutions with pH = 4, 7 and 10. In a typical release experiment 100 mg of MBT loaded containers were dispersed in 10 mL buffer solution and introduced into a dialysis tubing with a pore diameter of 6–8 nm (MWCO 50 kDa). The dialysis tubing was immersed in 240 mL buffer to ensure complete dissolution of the loaded MBT. The release medium and suspension in the dialysis tubing were vigorously stirred at room temperature to eliminate any possible particle agglomeration and release delay due to slow diffusion of MBT from the dialysis tubing to the release medium. Aliquots of 3 mL were taken from the release medium, followed by the addition of 3 mL fresh buffer solution at different time intervals for 24 h.

Coatings: The water-based organic coating is a two-component, model coating developed as a primer for aerospace applications by Mankiewicz GmbH. The resin component is an epoxy based primer, which consists of synthetic resins and water. The hardener component consists of polyamines in water. Water suspensions of the MBT loaded containers were added to the pre-mixed two components under stirring. The amount of water used to redisperse the containers prior to mixing with the paint was only 10 wt% of the paint and had no detrimental effect on the paint formulation. The following container fractions with respect to the cured coatings were embedded: 0.04, 0.2, 0.5, 0.7 and 1.7 wt%. The water-based organic primer was applied on AA2024-T3 plates using a spiral bar coater for 50 µm wet coating thickness. The coated samples were dried at 80 °C for 1 h after a flash-off time of 15 min at room temperature.

Characterization Methods: SEM (Zeiss Gemini LEO 1550) was employed to analyze the structure of silica containers as well as the

coated aluminium alloy substrates before and after the corrosion tests. SEM samples were sputtered with a gold/palladium mixture and analyzed at an operating voltage of 3 kV and different magnifications. TEM (Zeiss EM 912 Omega) was used to characterize the morphology, size and porous character of the synthesized silica containers. Thin slices of the SHS were obtained by embedding the silica powders in an epoxy matrix and cutting it with a microtome. The samples were investigated with an accelerating voltage of 120 kV. Analysis of the MBT concentration during release studies was performed with UV-Vis spectrometry (8453 UV-Visible spectrophotometer, Agilent Technologies) in the wavelength region 200–800 nm. Thermogravimetric analysis, TGA (NETZSCH TG 209 F1) was used to quantify the amount of loaded inhibitor in dried mesoporous silica containers. The TGA samples ($m \approx$ 10 mg) were exposed to a temperature increase from 25 °C to 1000 °C with a heating rate of 10 °C min^{-1} and the mass loss in a flow of oxygen (25 mL min^{-1}) was detected. Small-angle X-ray scattering (SAXS) measurements were conducted with dried, empty and MBT loaded silica containers, to investigate the pore structure and composition. SAXS profiles were recorded under vacuum on a Nanostar instrument (Bruker AXS, Karlsruhe, Germany) using Cu-Kα radiation with a wavelength of $\lambda = 0.154$ nm. A single photon counting area detector (HiStar, Bruker AXS) was used at a sample-detector distance of 25 and 105 cm and a range of scattering vector q from 0.1 to 7.5 nm^{-1} was covered. The pore structure and surface area of the silica containers were characterized with N_2 adsorption/desorption measurements (Micromeritics TriStar 3000) at –196 °C. Prior to the measurements the powder samples were baked under vacuum at 25 °C for 24 h. The surface area and pore size distribution were obtained from the N_2 isotherms by applying the BET (Brunauer-Emmett-Teller) theory and the NLDFT (non-local density functional theory) model for cylindrical pores considering the adsorption branch, respectively.

The coating thickness was measured with a coating thickness gauge (Surfix Pro S, from PHYNIX, Germany) using the Eddy-current principle and a coating thickness probe, FN1.5.[32] The dry adhesion tests were conducted with an electronically controlled hydraulic pump (PosiTest AT-A, DeFelsko), which was used to detach the pull-stubs glued to the freshly cured, coated samples.

The scanning vibrating electrode technique (SVET, Applicable Electronics) was used to analyze the active anticorrosive properties of the coated samples (1×2 cm^2) in 0.1 M NaCl solution. The coating was scratched (scratch length ≈ 2 mm) prior to the measurement to ensure exposure of the metal to the aggressive solution. The coated samples were then sealed with adhesive tape (Tesa, clear, 60 µm thickness) and only the area (3×3 mm^2) containing the scratch was left uncovered to ensure exposure to the NaCl solution. The exposed sample area was scanned every 15 min during 12 h with a vibrating Pt-blackened electrode tip (diameter of 20 µm) and the current density at 300 µm above the sample surface was detected.

In a typical EIS experiment, the coated substrates (6×3 cm^2) were placed into home-made cells, whereby an area of 3 cm^2 of the sample was exposed to 1 M NaCl solution at room temperature for 30 days. A three-electrode set-up was used and the impedance spectra were recorded at the open circuit potential. A reference (saturated calomel) and a counter (platinum) electrode were immersed in the cell. The coating at the edge of each sample was removed and the metal substrate, functioning as the working electrode, was connected to the potentiostat (CompactStat, Ivium Technologies). The current response was detected in the frequency range 100 kHz to 0.01 Hz at a constant potential (1 V) and a sinusoidal voltage signal of 10 mV. Six frequencies were typically assessed per decade. The spectra were obtained using the software Ivium Soft (release 1.985), normalized with the area of the working electrode (3 cm^2) and fitted with Zview.

The Machu test is an accelerated corrosion test, which is part of the specifications to obtain the QUALICOAT quality label for coatings on aluminium and aluminium alloy.[39] Prior to the test, a cross-cut incision (3×3 cm^2) with a width of 1 mm was introduced on coated aluminium panels with a scratch tool according to Sikkens to cut the coating down to the metal. The uncoated parts of the panels were isolated with adhesive tape. The test solution was a mixture of sodium chloride (50 g L^{-1}), 100% acetic acid (10 mL L^{-1}) and 30% hydrogen peroxide (5 mL L^{-1}) in water. The pH of the test solution was 3.0–3.3. The coated samples were immersed in the solution, the vials sealed and heated to 37 °C for 48 h. After 24 h, 5 mL L^{-1} of hydrogen peroxide (30%) were added. The pH of the test solution was also adjusted to 3.0–3.3 with glacial acetic acid, if needed. After the test, the area with the cross-cut was scratched and the area with removed coating around the scratch was examined. Photographs of the coated samples were taken before and after scratching over the cross-cut on the coated samples.

Supporting Information

Supporting Information is available from the Wiley Online Library or from the author.

Acknowledgements

The authors thank I. Zenke for SAXS measurements, R. Pitschke for TEM analysis, J. Tedim and K. Yasakau (CICECO, University of Aveiro, Portugal) for help with EIS data fitting. This work was financially supported by the FP7 "NanoBarrier" project of EU Commission and a German-Portuguese DAAD project.

Received: December 15, 2012
Published online: March 5, 2013

[1] M. L. Zheludkevich, R. Serra, M. F. Montemor, I. M. M. Salvado, M. G. S. Ferreira, *Surf. Coat. Technol.* **2006**, *200*, 3084.
[2] S. K. Ghosh, in *Self-healing materials fundamentals, design strategies, and applications*, (Ed. S. K. Ghosh), Wiley-VCH, Weinheim **2009**.
[3] S. K. Ghosh, in *Functional Coatings*, (Ed. S. K. Ghosh), Wiley-VCH Verlag GmbH & Co. KGaA, Weinheim **2006**, p. 1.
[4] D. G. Shchukin, D. O. Grigoriev, H. Möhwald, *Soft Matter* **2010**, *6*, 720.
[5] D. G. Shchukin, H. Möhwald, *Chem. Commun.* **2011**, *47*, 8730.
[6] J. R. Davis, *Corrosion: understanding the basics*, ASM International, Materials Park, OH **2000**.
[7] D. G. Shchukin, G. B. Sukhorukov, H. Möhwald, *Angew. Chem. Int. Ed.* **2003**, *42*, 4472.
[8] M. L. Zheludkevich, D. G. Shchukin, K. A. Yasakau, H. Möhwald, M. G. S. Ferreira, *Chem. Mater.* **2007**, *19*, 402.
[9] D. G. Shchukin, M. Zheludkevich, K. Yasakau, S. Lamaka, M. G. S. Ferreira, H. Möhwald, *Adv. Mater.* **2006**, *18*, 1672.
[10] D. O. Grigoriev, K. Kohler, E. Skorb, D. G. Shchukin, H. Möhwald, *Soft Matter* **2009**, *5*, 1426.
[11] E. V. Skorb, D. Fix, D. V. Andreeva, H. Möhwald, D. G. Shchukin, *Adv. Funct. Mater.* **2009**, *19*, 2373.
[12] D. Fix, D. V. Andreeva, Y. M. Lvov, D. G. Shchukin, H. Möhwald, *Adv. Funct. Mater.* **2009**, *19*, 1720.
[13] A. C. Balaskas, I. A. Kartsonakis, L. A. Tziveleka, G. C. Kordas, *Prog. Org. Coat.* **2012**, *74*, 418.
[14] M. J. Hollamby, D. Fix, I. Dönch, D. Borisova, H. Möhwald, D. Shchukin, *Adv. Mater.* **2011**, *23*, 1361.
[15] F. Maia, J. Tedim, A. D. Lisenkov, A. N. Salak, M. L. Zheludkevich, M. G. S. Ferreira, *Nanoscale* **2012**, *4*, 1287.
[16] A. Latnikova, D. Grigoriev, M. Schenderlein, H. Möhwald, D. Shchukin, *Soft Matter* **2012**, *8*, 10837.
[17] M. F. Haase, D. O. Grigoriev, H. Möhwald, D. G. Shchukin, *Adv. Mater.* **2012**, *24*, 2429.
[18] D. Borisova, H. Möhwald, D. G. Shchukin, *ACS Nano* **2011**, *5*, 1939.

[19] D. Borisova, H. Möhwald, D. G. Shchukin, *ACS Appl. Mater. Interfaces* **2012**, *4*, 2931.
[20] M. J. Hollamby, D. Borisova, H. Möhwald, D. Shchukin, *Chem. Commun.* **2012**, *48*, 115.
[21] M. Kruk, M. Jaroniec, *Chem. Mater.* **2001**, *13*, 3169.
[22] J. Wang, Y. Xia, W. Wang, M. Poliakoff, R. Mokaya, *J. Mater. Chem.* **2006**, *16*, 1751.
[23] M. J. Hollamby, D. Borisova, P. Brown, J. Eastoe, I. Grillo, D. Shchukin, *Langmuir* **2011**, *28*, 4425.
[24] F. Né, F. Testard, T. Zemb, I. Grillo, *Langmuir* **2003**, *19*, 8503.
[25] C. Urata, Y. Aoyama, A. Tonegawa, Y. Yamauchi, K. Kuroda, *Chem. Commun.* **2009**, 5094.
[26] M. Keppeler, J. Holzbock, J. Akbarzadeh, H. Peterlik, N. Hüsing, *Beilstein J. Nanotechnol.* **2011**, *2*, 486.
[27] K. Flodström, C. V. Teixeira, H. Amenitsch, V. Alfredsson, M. Lindén, *Langmuir* **2004**, *20*, 4885.
[28] J. M. Fedeyko, D. G. Vlachos, R. F. Lobo, *Langmuir* **2005**, *21*, 5197.
[29] Z. Zajíčková, C. Párkányi, *J. Heterocycl. Chem.* **2008**, *45*, 303.
[30] R. Woods, G. A. Hope, K. Watling, *J. Appl. Electrochem.* **2000**, *30*, 1209.
[31] U.S. Environmental Protection Agency. Hazard Characterization Document June 2010.
[32] J. Kral, R. Smid, H. M. G. Ramos, A. L. Ribeiro, presented at *Instrumentation and Measurement Technology Conference (I2MTC)*, **2011**, *IEEE* 10-12 May 2011, 2011.
[33] R. J. Bucci, C. J. Warren, E. A. Starke, *J. Aircr.* **2000**, *37*, 122.
[34] A. E. Hughes, A. Boag, A. M. Glenn, D. McCulloch, T. H. Muster, C. Ryan, C. Luo, X. Zhou, G. E. Thompson, *Corros. Sci.* **2011**, *53*, 27.
[35] J. He, V. J. Gelling, D. E. Tallman, G. P. Bierwagen, *J. Electrochem. Soc.* **2000**, *147*, 3661.
[36] S. V. Lamaka, M. Taryba, M. F. Montemor, H. S. Isaacs, M. G. S. Ferreira, *Electrochem. Commun.* **2011**, *13*, 20.
[37] C. H. Hsu, F. Mansfeld, *Corrosion* **2001**, *57*, 747.
[38] A. S. Castela, A. M. Simões, *Corros. Sci.* **2003**, *45*, 1631.
[39] QUALICOAT, http://www.qualicoat.net/qs_eng.asp 2012 (accessed September 2012).
[40] K. Möller, J. Kobler, T. Bein, *Adv. Funct. Mater.* **2007**, *17*, 605.
[41] Z. Teng, Y. Han, J. Li, F. Yan, W. Yang, *Microporous Mesoporous Mater.* **2010**, *127*, 67.